CrossMark

Crystallization kinetics of Li_2O–Al_2O_3–GeO_2–P_2O_5 glass–ceramics system

Anurup Das[1] · M. Goswami[1] · M. Krishnan[1]

Abstract

Lithium aluminum germanium phosphate glass–ceramics with NASICON structure find potential application in the field of energy storage device/solid-state battery. Two different glasses with nominal compositions (a) $Li_{1.5}Al_{0.5}Ge_{1.5}P_{2.9}Si_{0.1}O_{12}$ (LAGP1) and (b) $Li_{1.5}Al_{0.5}Ge_{1.5}P_{2.5}Si_{0.5}O_{12}$ (LAGP2) were prepared by standard melt-quench technique, and crystallization kinetics phenomenon in these systems was studied using differential thermal analysis technique (DTA). In addition to different conventional methods for crystallization kinetics analysis, model-free kinetics was also applied. The values obtained for activation energy of crystallization (E_a) are compared and used for determination of crystallization index, n and m. The E_a value obtained for LAGP1 is 375 ± 17 kJ mol^{-1} which is higher as compared to the E_a value of LAGP2, 199 ± 22 kJ mol^{-1}. LAGP2 with higher amount of Si(0.5) causes significant structural modification in the phosphate network and an early phase separation in the silico-phosphate glass. Thus, LAGP2 shows lower activation energy value as compared to LAGP1. The kinetic parameter, n, related to crystal nucleation, was evaluated from crystallized volume fraction (x) at a fixed temperature using predetermined E_a value, and other parameter 'm' related to the crystal growth was determined using the modified Kissinger equation. The model-free kinetics was used to evaluate the variation of E_a, m and n with temperature and suggests a dynamic nucleation and crystallization process with progressive change in kinetic parameters. In LAGP1 sample, an unusual increase in E_a value was observed at x value > 0.2 and can be correlated with the existing 'self-feeding' process, which is observed in DTA plots. In both of these systems, the values of n and m are found to be equal and more than 3 which suggests three-dimensional growths of $Li_{1.5}Ge_{1.5}Al_{0.5}(PO_4)$ crystals on a constant number of already grown nuclei. XRD and micro-Raman spectroscopy were used to identify the crystalline phase formed and various structural units present in the glass and glass–ceramics samples. Minor amount of $LiAlPO_4$ was confirmed from XRD and Raman spectroscopy along with major $Li_{1.5}Ge_{1.5}Al_{0.5}(PO_4)$ phase. In addition, using advanced kinetics and technology solution software non-isothermal data were simulated and the isothermal conversion data were extracted for various temperatures which are found to be very close to experimental isothermal data.

Keywords Solid-state electrolyte · Kinetic · Crystallization · Glass/glass–ceramics · Battery

Introduction

Glass–ceramics systems have several advantages over the glass systems in terms of their superior mechanical, thermal and electrical properties and can be tailor made for different applications. Glass–ceramics are prepared by either sintering route through surface nucleation or glass route, through bulk nucleation. In case of glass route, heat schedule for nucleation and crystallization in parent glass needs to be optimized, for acquiring desired crystalline phase and their appropriate concentration with correct microstructure. Many glass–ceramics are reported for potential applications in the field of optical, electrical, biomedical, nuclear, energy, consumer/domestics, etc. Among others, glass–ceramics with NASICON (acronym of Na Super Ionic Conductor) structure have potential application in the field of energy storage device specially in the form of Li–solid-state electrolyte in Li metal/Li-ion battery [1, 2]. In these systems, NASICON phase with an

✉ M. Goswami
   mgoswami@barc.gov.in

[1] Glass and Advanced Materials Division, Bhabha Atomic Research Centre, Trombay, Mumbai, India

open structure and large number of Li vacancy sites are responsible for high Li-ionic conductivity. In the literature, the glass ceramic systems based on $Li_2O–Al_2O_3–GeO_2–P_2O_5$ and $Li_2O–Al_2O_3–TiO_2–P_2O_5$ with NASICON phases are already reported for possible use as electrolyte in Li-ion battery. As desired crystalline phase with right microstructure is needed for achieving optimum electrical conductivity, chemical and thermal stability, thereby optimization of the process parameters is very much essential. Thus for developing new functional glass–ceramics materials, understanding the kinetics of nucleation/growth of glass system is considered as one of the most important step to control the desired properties during ceramization.

Differential thermal analysis (DTA) technique is one of the vital techniques to find out the kinetics of nucleation/growth. Although DSC technique is more accurate in measurements of heat of reaction as compared to DTA technique, many crystallization kinetics studies are reported using DTA technique with proper calibration. This is easy and comparatively reliable process to study on crystallization kinetics. DTA data are commonly used to optimize the process parameters, i.e., heating schedule for synthesizing many new functional glass–ceramics. In general, crystallization kinetics using DTA can be studied using either isothermal or non-isothermal kinetics with various established models [3, 4]. However, the non-isothermal one is relatively fast compared to the isothermal method. It is much more difficult to understand the nucleation/growth mechanism in the amorphous system as compared to other systems, i.e., metal or ceramic. The glass system needs better understanding due to complexity involved with multi-component system. Many times it is difficult to explicit the correct mechanism and employ a correct model to evaluate the kinetics parameters in the glass systems. Among many authors, Kissinger and Ozawa et al. [5, 6] studied extensively on crystallization kinetics and suggested that in simpler way the activation energy of crystallization (E_a) can be determined by non-isothermal process using Kissinger and Ozawa equations [7–10]. However, these methods are not appropriate to apply in the amorphous system where crystallization is followed by nucleation and growth rather than nth-order kinetic reaction. These methods encounter with an error in activation energy calculation and give no information about the nucleation and growth mechanism. Although many studies related to kinetics of different glass systems are reported, these always included error because of the many approximations. In addition to non-isothermal kinetics, many authors used isothermal crystallization kinetics to evaluate E_a and kinetics parameters [11–13]. John–Mehl–Avrami (JMA) equation is primarily based on isothermal crystallization, but many authors also used JMA equation for non-isothermal crystallization kinetics study

[14–16]. Later on, Matusita et al. [3] proposed non-isothermal crystallization kinetics on taking account of nucleation and growth mechanism and calculated the activation energy. This method is found more suitable for glass and glass–ceramic systems. For Avrami exponent determination, some authors used FWHM of the DTA peak employing Ozawa equation [17, 18]. Nowadays, the model-free kinetics, based on iso-conversional methods, became much popular because these are found to be more accurate [19–21]. The calculation of activation energy based on iso-conversional method does not require knowledge of growth mechanism and has less number of approximations. In a recent communication uses of linear iso-conversional methods, Kissinger–Akahira–Sunose (KAS) method, Starink method and Tang method to calculate the activation energy of crystallization are reported [22, 23]. Few studies on the crystallization kinetics of similar $Li_2O–Al_2O_3–GeO_2–P_2O_5$ system are also reported where calculation of activation energy of crystallization using various methods is carried out [24–26].

Although many studies are reported on $Li_2O–Al_2O_3–GeO_2–P_2O_5$ systems on various aspects of these materials for improved performance in solid-state battery, study on crystallization kinetics with the effect of other network former, i.e., SiO_2, is not reported. In the present work, we aim to carry out a comparative crystallization kinetics study in two different $Li_2O–Al_2O_3–GeO_2–P_2O_5$ (LAGP) glass–ceramics systems with effect of different P_2O_5/SiO_2 contents. As these systems have potential application in the field of energy storage device, this need right amount of NASICON phase with desired microstructure for optimum performance. In this study, SiO_2 was substituted in place of P_2O to see the improvement in the chemical stability of the system. Various methods are used to evaluate the kinetic parameters and understand the growth and kinetics in these systems. E_a obtained from model-free kinetics is used to evaluate the kinetics parameters (m and n). Isothermal data were simulated from non-isothermal data, using AKTS (advanced kinetics and technology solution software) [27]. X-ray diffractometer (XRD) and micro-Raman spectroscopy were used to identify the nature of phases and different structural units present in the glass and glass–ceramics samples.

Experimental

Two different glass systems with compositions (a) $Li_{1.5}Al_{0.5}Ge_{1.5}P_{2.9}Si_{0.1}O_{12}$ (LAGP1) and (b) $Li_{1.5}Al_{0.5}Ge_{1.5}P_{2.5}Si_{0.5}O_{12}$ (LAGP2) were prepared by standard melt-quenched technique. Each 100 g of batches was prepared by taking initial constituents, in the form of carbonate and diammonium hydrogen phosphate of proportionate

amount. Initial batch was calcined at their corresponding decomposition temperatures and held for sufficient time to convert into their corresponding oxide form. The calcinations process was repeated to ensure complete decomposition after through mixing and grinding. After calcination, the charge was mixed and grounded properly and melted in a Pt–Rh crucible at around 1450–1550 °C. The melt was held at the melting temperature for 1–2 h for homogenization and poured on a metal plate. The glass was annealed at around 450–550 °C for 4–6 h and cool down to room temperature slowly.

The annealed glasses were powdered, and differential thermal analysis measurements were carried out using a TGA/DTA instrument, Model Labsys 1600, M/s Setaram, France. Pt crucible was used as both sample and reference. Solid glass samples were taken for the DTA scan to avoid the dependency of crystallization on the particle size distribution. The measurements were carried out using air as carrier gas with a flow rate of 70 L min^{-1}. For kinetics measurements, DTA scans were recorded at the heating rates of 5, 10, 15, 20 and 25 K min^{-1}. The samples were scanned up to maximum 900 °C. Area under the DTA curve was calculated after proper baseline correction. AKTS (advanced kinetics and technology solution) software was used for simulation of non-isothermal data and model-free kinetics prediction. Powder X-ray diffraction (XRD) technique was used to identify the nature of crystalline phases present in these glass–ceramics (GC) samples using a Bruker D8 Discover instrument with collimated CuKα radiation source. Micro-Raman spectroscopy was studied using a micro-Raman instrument model: Invia-Reflex (M/s Renishaw, UK) with 532-nm laser source.

Theoretical consideration

Isothermal crystallization

Isothermal kinetics was mainly introduced by John, Mehl and Avrami (JMA), and the equation used for kinetic analysis is

$$x(t) = 1 - \exp(-kt)^n \tag{1}$$

where x is crystallized volume fraction at a fixed temperature in time t, n is Avrami parameter and k is reaction rate [28]. After taking logarithm on both sides, the above expression can be rewritten as,

$$\ln[-\ln(1-x)] = n\ln t + n\ln k \tag{2}$$

Equation (2) will give a straight line by plotting $\ln[-\ln(1-x)]$ versus $\ln t$. Slope of the above straight line gives the value of 'n.' Theoretically, n value will be 4.0 when whole volume of glass sample participates in

crystallization with three-dimensional spherical growths. But the n value can also vary from 1.0 to 4.0 depending upon the dimensionality of growth.

Non-isothermal crystallization

This is the most common method used for determination of the activation energy of crystallization. The peak crystallization temperatures, which increase with increasing rate of heating, are considered to determine the value E_a using Kissinger's or Ozawa's equation. These methods are not suitable where the crystallization mechanism is through nucleation and growth process. Later, Matusita et al. [3] and Augis and Bennett reported the non-isothermal kinetics study of amorphous material based on crystal nucleation and growth.

For the glass samples containing large number of nuclei, N can be taken as constant, whereas N will be inversely proportional to β, if before the DTA run there are no nuclei. In general, for non-isothermal crystallization, the crystallized volume fraction (x) is related to the heating rate (β) by the following equation which can be derived using Doyle's p-function [29]

$$\ln[-\ln(1-x)] = \ln A_1 + 2n\ln T - n\ln\beta - \frac{mE_a}{RT} \tag{3}$$

where m represents the dimensionality of crystal growth and its value changes from 1 to 3. For N varies with temperature, the $n = m + 1$ and $n = m$ when N is constant. The second term in the right-hand side of Eq. (3) can be taken as constant because natural logarithm of T, at higher values, does not change significantly. Using a better approximation [6], the above equation can be rewritten as

$$\ln[-\ln(1-x)] = \ln A_2 - n\ln\beta - 1.052\frac{mE_a}{RT} \tag{4}$$

$$\text{Or, } \ln\beta = \ln A_2 - 1.052\frac{mE_a}{nRT} - \frac{1}{n}\ln[-\ln(1-x)] \tag{5}$$

The above expression also known as modified Ozawa equation. Theoretically, the parameter, n, related to crystal nucleation, can be calculated from the slope of $\ln[-\ln(1-x)]$ versus $\ln\beta$ plot at a specific temperature. At peak crystallization temperature, the value of x is independent of rate of heating. Though the activation energy of crystallization is not constant throughout the transformation, E_a can be calculated at $T = T_P$, from $\ln\beta$ versus $\frac{1}{T_P}$ plot, assuming $n = m$, and N is constant in Eq. (5).

So, the value of n cannot be calculated precisely using Eqs. (3) and (4) because in these equations E_a is not constant, but practically, it is a function of x.

The rate of change of x reaches its maximum at $T = T_P$. Equation (4) can be solved taking $\frac{d}{dt}\left(\frac{dx}{dt}\right) = 0$, and the following equation can be derived [3] as

$$\ln\left(\frac{\beta^n}{T_P^2}\right) = -1.052m\frac{E_a}{RT_P} + \text{constant} \qquad (6)$$

where T_P is the peak crystallization temperature in absolute scale. Value of m can be calculated from the slope of $\ln\left(\frac{\beta^n}{T_P^2}\right)$ versus $\frac{1}{T_P}$ plot after knowing the values *of* n and E_a accurately is known as modified Kissinger plot.

Model-free kinetics

Model-free iso-conversional methods are most reliable for determination of apparent E_a of a thermally simulated complex kinetics process. Generally, iso-conversional methods can be classified into two categories, integral and differential [30]. These methods can be used to simulate isothermal data from non-isothermal data and help to compute conversion-time curve at a fixed temperature. In this study, integral iso-conversional method is followed to determine the apparent activation energy E_a.

Integral iso-conversional method

This method is also called as Ozawa–Flynn–Wall [31, 32] method. It is assumed that the rate of conversion $\frac{dx}{dt}$ is a linear function of reaction rate, $k(T)$, and a function of x, which is temperature independent

$$\frac{dx}{dt} = k(T)f(x) \qquad (7)$$

For a fixed conversion (x)

$$\ln\beta = \ln\left[\frac{k_0 E}{R}\right] - \ln g(x) - 5.3305 - 1.052\frac{E_a}{RT} \qquad (8)$$

By using Eq. (8), the plot of $\ln\beta$ versus $\frac{1}{T}$, E_a can be evaluated from the slope at a particular conversion. The method to determine E_a using Eqs. (5) and (8) is also known as model-free kinetics.

Results

Thermal stability

In general, crystallization tendency of a glass system can be predicted from the glass stability factor. This can be easily estimated from the glass transformation temperature (T_g) and crystallization temperature (T_c) obtained from DTA, using the equation as given below [33, 34].

$$\Delta T = T_c - T_g \qquad (9)$$

$$\text{Or } \Delta T' = \frac{T_c - T_g}{T_g} \qquad (10)$$

where T_c is the onset of glass crystallization temperature and T_g is the glass transition temperature. Various thermal parameters obtained from DTA measurements for LAGP1 and LAGP2 are summarized in Table 1.

Crystallization kinetics

From Table 1, the preliminary information about the stability of these glass systems are evaluated. Further crystallization kinetics in detail is carried out using different DTA scans. Non-isothermal kinetics has been used to evaluate the activation energy in these glass systems prior to determination of kinetics parameters m and n. Although many equations/models are used to estimate E_a values, it is a challenge to find out appropriate kinetics applicable to individual systems which helps to predict correctly all kinetics parameters.

Figures 1 and 2 show the DTA scans recorded at different heating rates for LAGP1 and LAGP2, respectively. The figures show onset of a broad endotherm at around 550 °C indicating glass transition temperature for LAGP1, which is observed to be higher compared to glass transition temperature (~ 500 °C) of LAGP2. This endotherm is followed by one very sharp and intense exothermic peak, indicating crystallization temperature (T_p) at around 675 and 575 °C for LAGP1 and LAGP2, respectively. With increase in scan rate from 5 to 20 K min^{-1}, the T_c shifted to higher temperature, from 596 to 614 °C for LAGP1 and from 578 to 613 °C for LAGP2. In addition, a small loop was observed at the middle of the exothermic peak in the DTA scan of LAGP1 which suggests existing of certain 'self-feeding' reaction, in this system [35]. It suggests existence of some endothermic reaction along with the crystallization process and the reaction subdue and baseline comes to equilibrium as soon as the crystallization over.

Table 1 Various thermal parameters obtained from DTA

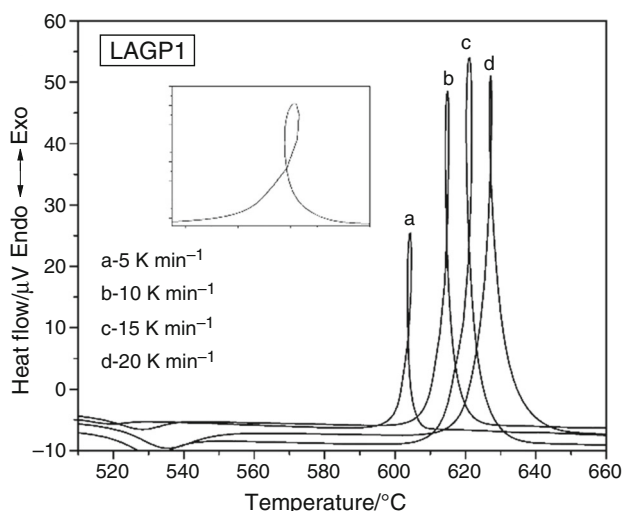| Sample name Rate of heating/ K min^{-1}	LAGP1				LAGP2			
	$T_g/$ °C	$T_c/$ °C	$T_P/$ °C	$T_c - T_g/$ °C	$T_g/$ °C	$T_c/$ °C	$T_P/$ °C	$T_c - T_g/$ °C
5	508	596	604	88	472	578	590	106
10	513	604	614	91	477	594	607	117
15	516	609	621	93	482	604	617	122
20	520	614	627	94	486	613	632	127

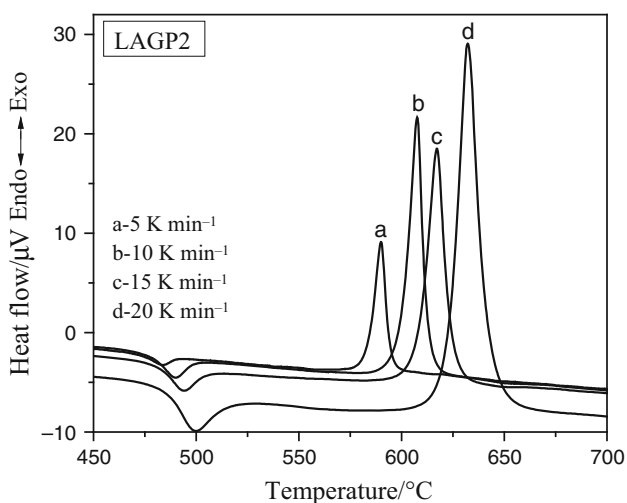**Fig. 1** DTA scans for LAGP1 at different heating rates

Fig. 2 DTA scans for LAGP2 at different heating rates

Determination of activation energy of crystallization (E_a)

According to Augis and Bennett [36], calculation of activation energy of crystallization (E_a) can be done in amorphus system using the peak crystallization temperatures obtained from DTA scans recorded at different heating rates, 5, 10, 15 and 20 K min^{-1}. The equation used for determination of E_a is given as below.

$$\ln\left(\frac{\beta}{T_P}\right) = -\left(\frac{E_a}{RT_P}\right) + \text{constant} \tag{11}$$

where β is the rate of heating and T_P is the peak crystallization temperature.

Figure 3 shows the plot of $\ln\left(\frac{\beta}{T_P}\right)$ versus $\frac{1}{T_P}$ for LAGP1 and LAGP2 samples, and the E_a values are calculated from the slope of the plot.

As reported previously by Matusita and Sakka [14], that the crystal volume fraction (x) can be calculated from the area under the DTA curve, as it is equivalent to the area fraction.

Figures 4 and 5 show the variation of crystal volume fraction (x) with temperature for different heating rates for LAGP1 and LAGP2, respectively. Using the plots $\ln \beta$ versus $\frac{1}{T}$, the activation energies at different stages of reaction progress were calculated. The calculated E_a values are plotted with respect to fraction of crystallization in Figs. 6 and 7 for LAGP1 and LAGP2, respectively. From
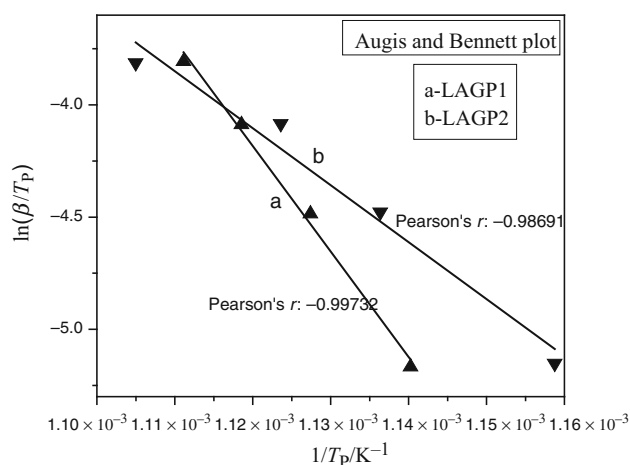
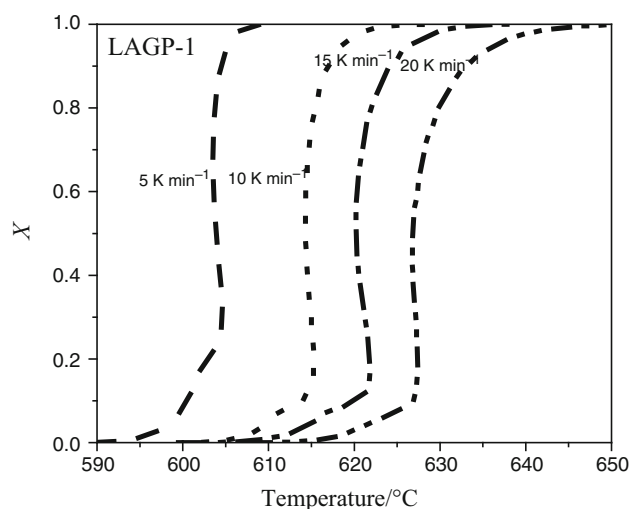

Fig. 3 Augis and Bennett activation energy plot

Fig. 4 Experimental crystallized volume fraction (x) versus temperature plots at different rates of heating for LAGP1
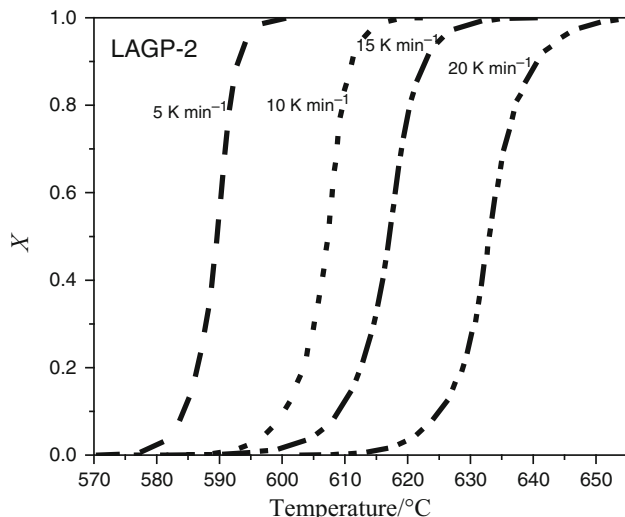
Fig. 5 Experimental crytallized volume fraction (x) versus temperature plots at different rates of heating for LGAP2
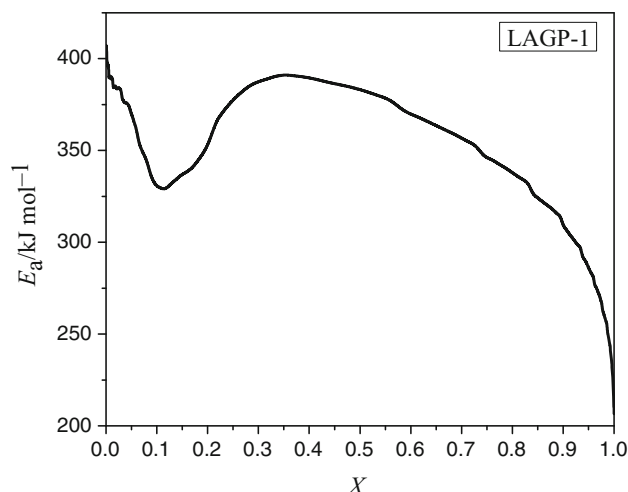

Fig. 6 E_a versus crystallized volume fraction (x) plot for LAGP1

the figures, it is observed that E_a is varying significantly at initial and final phase of crystallization. It is seen that the activation energy calculated at different crystallized fractions has an associated error and this error is usually higher at low crystalline fraction. This is because of the difficulty in measurement of small area under the peak for determining the crystallization volume fraction, x at initial stage of crystallization [28]. In addition, in Fig. 6, there is a significant increase in E_a for $x > 0.2$ fraction of crystal volume, which may be due to the self-feeding of the sample as shown in Fig. 1. In self-feeding, the energy released by the system was taken back and the energy become insufficient to overcome the barrier of crystallization and thus increased the E_a value.

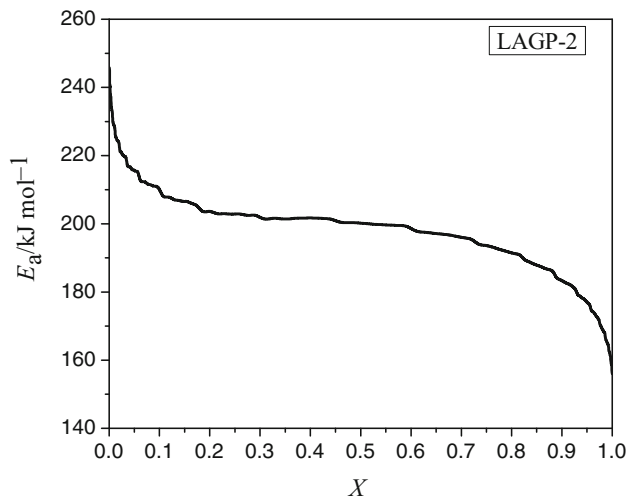For model-free kinetics analysis using the iso-conversion method, activation energy at peak crystallization

Fig. 7 E_a versus crystallized volume fraction (x) plot for LAGP2

temperature was calculated using Eq. (5), where x was kept fixed. Figure 8 shows the plot of $\ln \beta$ versus $\frac{1}{T_P}$, for LAGP1 and LAGP2, and the slope of this plot gives the value of E_a (Table 2). The E_a value obtained is nearly same as calculated from Augis and Bennett plot. The value further well coincides with the value obtained from integral iso-conversional method for $x \sim 0.5$. The E_a value obtained from all different plots is compared in Table 2 and used for calculation of 'm' as given below.

Determination of the kinetic parameters (n and m)

For different heating rates, fraction of conversion (x) is different at a fixed temperature, and for the $\ln[-\ln(1 - x)]$ versus $\ln\beta$ plot, the x versus temperature plots should be
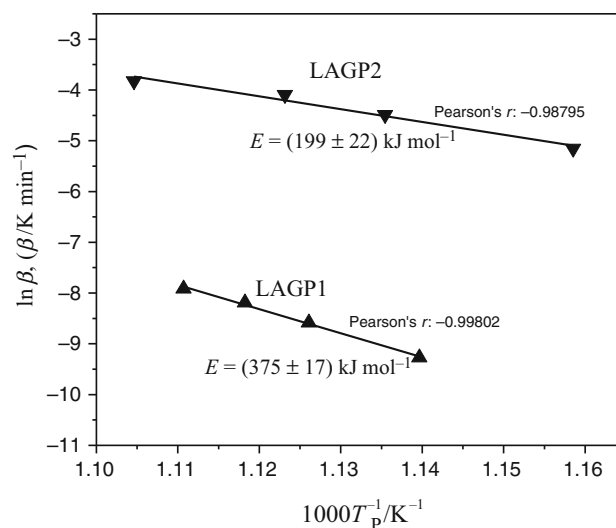

Fig. 8 $\ln \beta$ versus $\frac{1}{T_P}$ plot to evaluate E_a for LAGP1 and LAGP2

Table 2 Values of activation energies of crystallization obtained from different plots

Sample name	Activation energy of crystallization (E)/kJ mol^{-1}			Kinetics parameters	
	Augis and Bennett plot $\ln\frac{\beta}{T_P}$ versus $\frac{1}{T_P}$	Modified Ozawa-type plot $\ln\beta$ versus $\frac{1}{T_P}$	Model-free kinetics (integral iso-conversional method) (x = 0.2–0.8)	n	m
LAGP1	(391 ± 20)	(375 ± 17)	(372.75 ± 0.34)	3.17 ± 0.15 (at T = 599 °C)	2.99 ± 0.15 (at T = 599 °C)
				2.16 ± 0.07 (at T = 588 °C)	1.98 ± 0.10 (at T = 588 °C)
LAGP2	(211 ± 24)	(199 ± 22)	(198.87 ± 0.08)	3.12 ± 0.22 (at T = 589 °C)	3.06 ± 0.35 (at T = 589 °C)
				2.19 ± 0.08 (at T = 585 °C)	2.01 ± 0.23 (at T = 585 °C)

closed enough with respect to temperature axis so that at a fixed temperature, different values of x can be extracted. For this, we have used AKTS software to simulate the crystallized volume fraction data (x) with respect to temperature at the heating rates of 10, 11, 12 and 13 K min^{-1} which is shown in Figs. 9 and 10, for LAGP1 and LAGP2, respectively. Equation (4) has been used for estimation of 'n,'. Figures 11 and 12 show the plot of $\ln[-\ln(1-x)]$ versus $\ln\beta$, for LAGP1 and LAGP2 at two different temperatures. The slope gives the value of n. Similarly, the 'm' value is calculated from modified Kissinger plots as shown in Figs. 13 and 14. These figures show the values of 'm' for LAGP1 and LAGP2 at two different temperatures, and it is observed that the value changes with temperature similar to 'n.' To calculate 'm' value from the slope, E_a value was taken as (375 ± 17) and (199 ± 22) kJ mol^{-1} for LAGP1 and LAGP2, respectively, which is obtained from model-free analysis. Values of n and m obtained for different
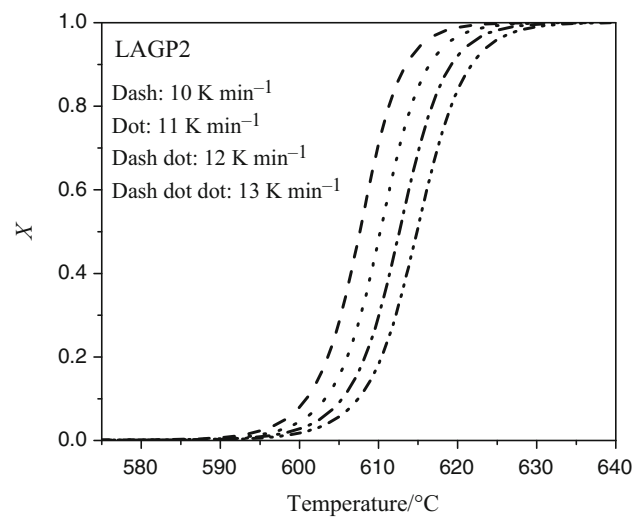
Fig. 10 Simulated crystallized volume fraction (x) versus temperature plots at different rates of heating for LAGP2
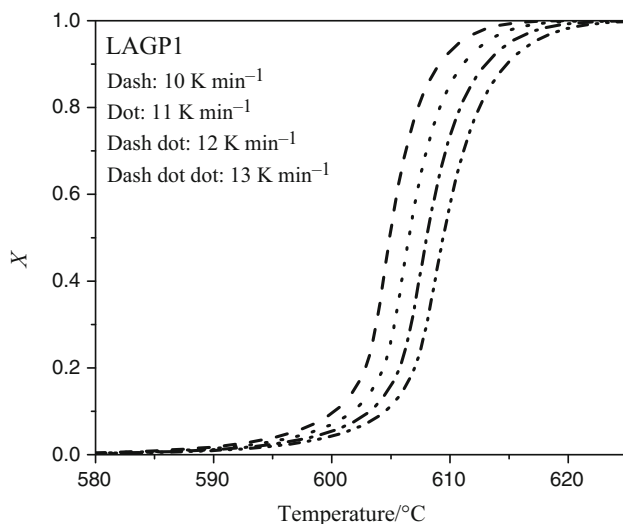
Fig. 9 Simulated crystallized volume fraction (x) versus temperature plots at different rates of heating for LAGP1
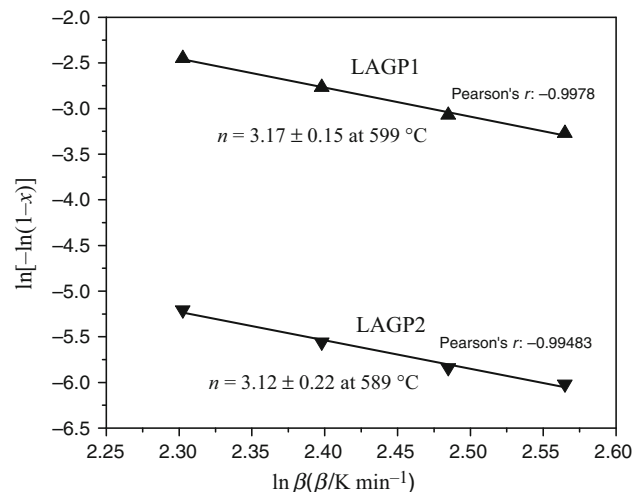
Fig. 11 $\ln[-\ln(1-x)]$ versus $\ln\beta$ plots for LAGP1 at 599 °C and LAGP2 at 589 °C
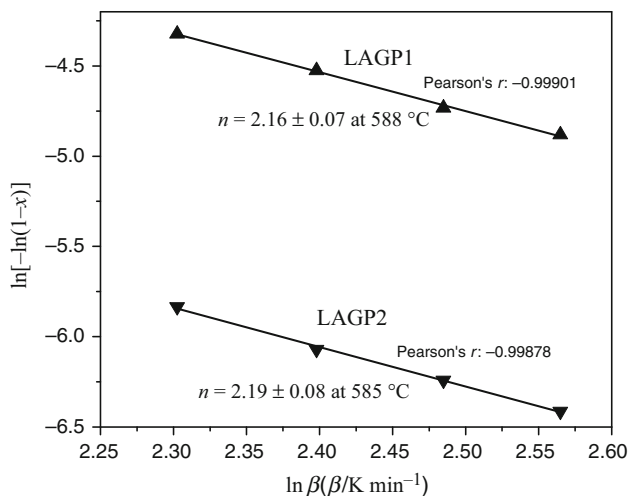
Fig. 12 $\ln[-\ln(1-x)]$ versus $\ln\beta$ plots for LAGP1 at 588 °C and LAGP2 at 585 °C

Fig. 14 Modified Kissinger plot for LAGP1 and LAGP2 at taking $n = 2.0$

Fig. 13 Modified Kissinger plot for LAGP1 and LAGP2 taking $n = 3.0$
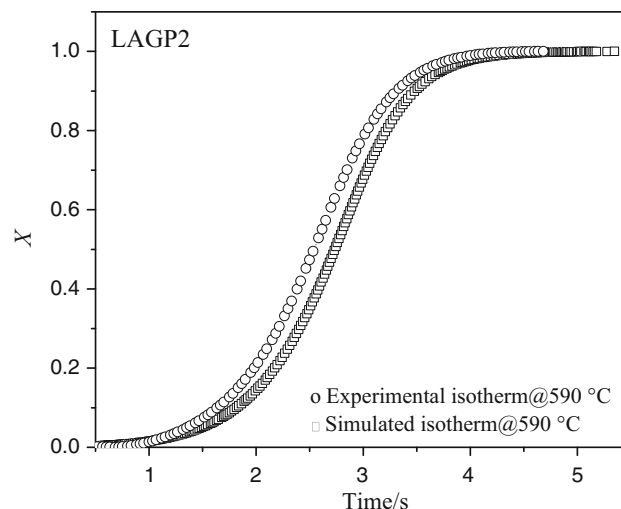
Fig. 15 Simulated and experimental plot of x versus time (t) for LAGP2

temperatures for both LAGP1 and LAGP2 are summarized in Table 2.

Simulation of isothermal data from non-isothermal data

AKTS software is used to simulate isothermal conversion fraction (x) with respect to time with non-isothermal data input. Figure 15 shows the comparative plot of x versus time (t) obtained from simulated and experimental data for LAGP2 sample. Simulated data obtained almost follow the experimental data within error. Reaction progress prediction at any temperature was simulated using the software.
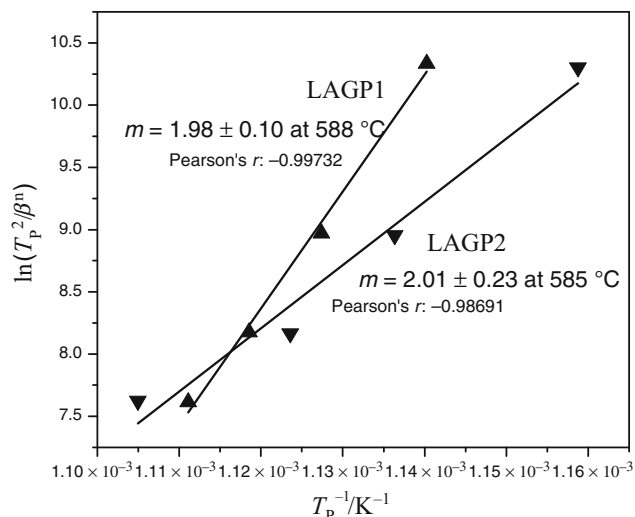
Phase identification by XRD

Figure 16 shows the merged XRD plots of LAGP1 and LAGP2 glass–ceramics samples. Formation of $LiGe_2(PO_4)_3$ phase in both LAGP1 and LAGP2 GC sample is confirmed from the figures. In addition, the figure shows the presence of minor impurity phase of $LiAlPO_4$ along with major NASICON phase $[LiGe_2(PO_4)_3]$ phase in LAGP2 sample.

Structural studies using micro-Raman spectroscopy

Figures 17 and 18 show the Raman spectra of LAGP1 and LAGP2 glass and glass–ceramics, respectively. Figure 16
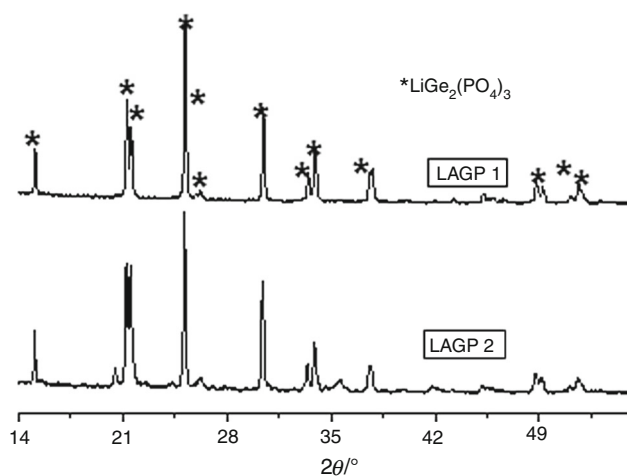
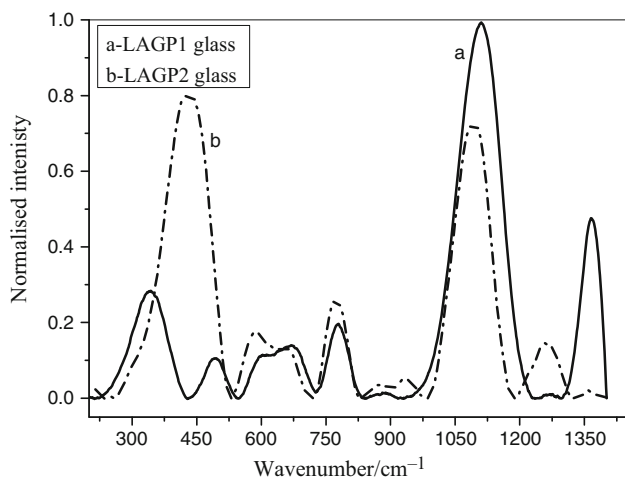Fig. 16 XRD plots of LAGP1 and LAGP2 glass–ceramics

Fig. 17 Raman spectra LAGP1 and LAGP2 glasses

Fig. 18 Raman spectra of LAGP1 and LAGP2 glass–ceramics

Discussion

LAGP2 with higher amount of SiO$_2$ has higher glass stability factor as compared to LAGP1 (Table 1), which indicates lesser tendency toward crystallization. With the addition of SiO$_2$, the strength of the glass network increases and glass transition/viscosity increases for the system because of formation of Si(6) structural units [41]. It is also observed that the glass stability factor increases with increase in rate of heating. The higher shift in glass transition and crystallization temperature is because the system does not get sufficient temperature with increase in rate of heating and get delayed in the initiation of glass transformation or onset of crystallization process. The E_a values obtained are (391 ± 20) and (211 ± 24) kJ mol^{-1} for LAGP1 and LAGP2, respectively. Similar values are also obtained by pure LAGP system [24–26]. In case of LAGP2, the presence of large amount of SiO$_2$ in P$_2$O$_5$ network causes possible phase separation at early stage of heating and reduces the barrier for growth and thus has lower E_a. According to Eqs. (5) and (8), E_a varies with progress of crystallization/conversion and the values of activation energy are different at different temperatures [19, 20]. This implies that crystallization process in glass–ceramics is a complex and multi-step process [21]. Using model-free kinetics, E_a at different temperatures was calculated and plotted against the conversion factor x. Table 2 shows that E_a values obtained from different methods match with each other. The value obtained from Augis and Bennett plot and modified Ozawa plot is a fixed value for entire range of the temperature, whereas the E_a value, obtained from model-free kinetics analysis, is much more accurate and the value is taken here for the calculation of crystallization index m and n. The E_a values obtained from model-free method are calculated from the average E_a obtained in the region of $x = 0.2$–0.8.

shows prominent signature of SiO$_2$ bands in the region of 440 and 100–1200 cm^{-1} for LAGP2 glass sample. One additional band at 1350 cm^{-1} is seen in LAGP1 glass sample which indicates the presence of P=O terminal of P(3) units [37–40]. One broad band in the region of 1200–1350 cm^{-1} in LAGP2 glass is because of the presence phospho-silicate (-P–O–Si–) structural units, which are almost absent in LAGP1 glass. The presence of stretching vibration of Ge–O in GeO$_6$ structural units is confirmed from the band positioned in the region of 650 cm^{-1} in case of both the samples. Bands shown at 723 and 1042 cm^{-1} are for P–O–Si band which are more prominent in LAGP2 sample. In case of glass ceramic samples, more number of sharp peaks are observed in LAGP2 as compared to LAGP1, which indicates the presence of additional phases, i.e., silicate and phosphate phases along with major NASICON phase in glass–ceramics sample.
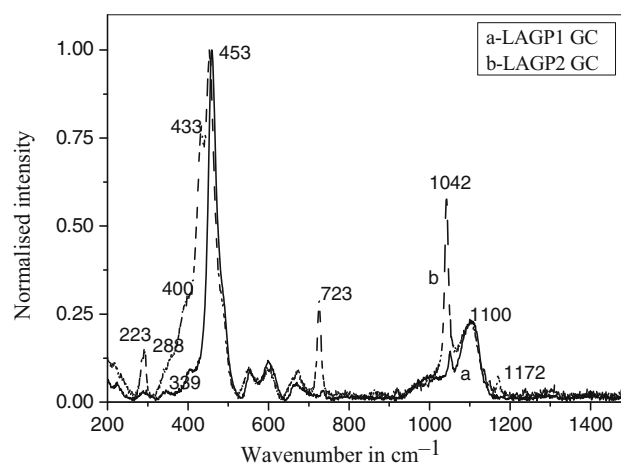
It is also observed that the value of 'n' calculated from the slope of Figs. 11 and 12 is not constant at any temperature, but it increases, with increase in temperature. At low temperature (~ 580 °C), the value of n is nearly 2.0, and at higher temperature (~ 598 °C) the value of n is 3.0. The n value can be maximum 3.0 or 4.0 depending on whether the glass is quenched or preannealed for a constant number of nuclei. The value 3.0 and more also indicate a bulk nucleation/crystallization in the glass. In both the systems, the values of n and m found to be same. This implies that large number of nucleus are already exist before the DTA scan and the value do not change much with respect to temperature during DTA measurement. The reason behind the variation of 'm' values with temperature is because of the progressive growth of the nuclei with different morphologies at different temperature spans. Initially, the crystal particles start to grow in like a rod shape in one dimension and then become spherical shape, and after that, they interconnect to each other and individual particle shape could not be distinguished. Raman spectra also show increase in strength in glass network in LAGP2 samples because of higher SiO_2 content and also formation of different crystalline phases in glass ceramic sample. Because of double bond in phosphate network, there is a strain in the structure of the phosphor-silicate glass network and causes the phase separation at the early stage of heating. For LAGP1 sample, the crystallization temperature is much higher which indicates the processing temperature of LAGP1 is high, whereas for LAGP2, NASICON phase grows at lower temperature and additional impurity phases were seen to formed at higher temperature. The formation of $LiGe_2(PO_4)_3$ along with minor $LiAlPO_4$ is confirmed from XRD and Raman spectroscopy.

Conclusions

Two LAGP (lithium aluminum germanium phosphate) system with compositions (a) $Li_{1.5}Al_{0.5}Ge_{1.5}P_{2.9}Si_{0.1}O_{12}$ and (b) $Li_{1.5}Al_{0.5}Ge_{1.5}P_{2.5}Si_{0.5}O_{12}$ are studied for comparative crystallization kinetics using DTA technique. Non-isothermal kinetics was studied using different equations and model-free kinetics for determination of activation energy. The activation energy (E_a) values obtained from various methods are comparable. Higher value of E_a (375 ± 17 kJ mol^{-1}) for LAGP1 was obtained as compared to LAGP2 (199 ± 22 kJ mol^{-1}). This is because higher SiO_2 content in LAGP2 causes more asymmetry in network structure and initiates phase separation at low temperature. On the other hand, n and m of value ≥ 3.0 clearly indicate the three-dimensional growth of LAGP phase followed by growth due to interdiffusion process at

higher temperature. Equal value of n and m also confirms the presence of large number of nuclei before the crystal growth. The activation energy and kinetics parameters are found to be temperature dependent and vary with temperatures. The E_a values varied significantly at low fraction of conversion factor (x) and remain almost constant at higher value of x. For LAGP1, the value of E_a varies significantly as compared to LAGP2. This suggests some inherent chemical reaction/rearrangement causing an increase in the barrier for crystallization of NASICON phase in LAGP1 sample. Isothermal data simulated from non-isothermal data using AKTS software are within the error of experimental data. LAGP1 shows lesser number of additional minor impurity phases than LAGP2 and shows higher chemical stability and found more suitable for use as electrolyte.

References

1. Wang Y, Richards WD, Ong SP, Mara LJ, Kim JC, Mo Y, Ceder G. Desgin principles for solid-state lithium superionic conductors. Nat Mater. 2015;. https://doi.org/10.1038/NMAT4369.
2. Bates JB, Dudney NJ, Neudecker B, Ueda A, Evans CD. Thin-film lithium and lithium-ion batteries. Solid State Ion. 2000;135:33–45.
3. Matusita K, Komatsu T, Yokota Y. Kinetics of non-isothermal crystallization process and activation energy for crystal growth in amorphous materials. J Mater Sci. 1984;19:291–6.
4. Avrami M. Granulation, phase change, and microstructure kinetics of phase change. III. J Chem Phys. 1941;9:177.
5. Kissinger HE. Reaction kinetics in differential thermal analysis. Anal Chem. 1957;29:1702–6.
6. Ozawa T. Kinetic analysis of derivative curves in thermal analysis. J Therm Anal. 1970;2:301–24.
7. Kasprzyk M, Sroda M, Szumera M. Influence of Gd_2O_3 on thermal stability of oxyfluoride glasses. J Therm Anal Calorim. 2017;130:207–20.
8. Davim EJC, Senos AMR, Fernandes MHV. Non-isothermal crystallization kinetics of a Si–Ca–P–Mg bioactive glass. J Therm Anal Calorim. 2014;117:643–51.
9. Sinouh H, Bih L, Manoun B, Lazor P. Thermal analysis and crystallization of the glasses inside the $BaO–SrO–TiO_2–NaPO_3$ system. J Therm Anal Calorim. 2017;128:883–90.
10. Basaran C, Canikoglu N, Toplan HO, Toplan N. The crystallization kinetics of the $MgO–Al_2O_3–SiO_2–TiO_2$ glass ceramics system produced from industrial waste. J Therm Anal Calorim. 2016;125:695–701.
11. Johnson WA, Mehl RF. Reaction kinetics in processes of nucleation and growth. Trans AIME. 1939;135:396–415.
12. Avrami M. Kinetics of phase change. I general theory. J Chem Phys. 1939;7:1103–12.
13. Avrami M. Kinetics of phase change. II transformation-time relations for random distribution. J Chem Phys. 1940;8:812–24.
14. Matusita K, Sakka S. Kinetic study of the crystallization of glass by differential scanning calorimetry. Phys Chem Glasses. 1979;20:81–4.
15. Golz J. Crystallization of glassy $2PbO\cdot SiO_2$ studied by DTA. Phys Chem Glasses. 1977;18:32–5.

16. Marseglia EA. Kinetic theory of crystallization of amorphous material. J Non Cryst Solids. 1980;41:31–6.

17. Wang HY, He K, Zu KC, Chen J. Study on crystallization kinetics of Li$_2$O–Al$_2$O$_3$–GeO$_2$–P$_2$O$_5$ glass by non-isothermal technique. Adv Mater Res. 2012;535–537:1629–33.

18. Wang J, Lio C, Zhang G, Xie J, Han J, Zhao X. Crystallization properties of magnesium aluminosilicate glass–ceramics with and without rare-earth oxides. J Non Cryst Solids. 2015;419:1–5.

19. Khawam A, Douglas R, Flanagan DR. Role of isoconversional methods in varying activation energies of solid-state kinetics II. Nonisothermal kinetic studies. Thermochim Acta. 2005;436:101–12.

20. Pacurariu C, Lazau RI, Lazau I, Ianos R, Tita B. Non-isothermal crystallization kinetics of some basaltic glass–ceramics containing CaF$_2$ as nucleation agent. J Therm Anal Calorim. 2009;97:507–13.

21. Vlase T, Pacurariu C, Lazau RI, Lazau I. Kinetic studies of the crystallization process of glass–ceramics based on basalt. J Therm Anal Calorim. 2007;88:625–9.

22. Pacurariu C, Lazau I. Non-isothermal crystallization kinetics of some glass–ceramics with pyroxene structure. J Non Cryst Solids. 2012;358:3332–7.

23. Starink MJ. Activation energy determination for linear heating experiments; deviation due to neglecting the low temperature end of the temperature integral. J Mater Sci. 2007;42:483–9.

24. Kun H, Yanhang W, Chengkui Z, Huifeng Z, Yonghua L, Jiang C, Bin H, Juanrong M. Influence of Al$_2$O$_3$ additions on crystallization mechanism and conductivity of Li$_2$O–GeO$_2$–P$_2$O$_5$ glass–ceramics. Physica B. 2011;406:3947–50.

25. Rodrigues AM, Narváez-Semanate JL, Cabral AA, Rodrigues ACM. Deteremination of crystallization kinetics parameters of a Li$_{1.5}$Al$_{0.5}$Ge$_{1.5}$(PO$_4$)$_3$ (LAGP) glass by differential scanning calorimetry. Mater Res. 2013;16:811–6.

26. Kun H, Yanhang W, Chengkui Z, Yonghua L, Huifeng Z, Bin H, Jiang C. Crystallization kinetics of lithium aluminum germanium phosphate glass by DSC technique. J Wuhan Univ Technol Mater Sci Ed. 2012;27:63–6.

27. Mohoric I, Krajnc M, Sebenik U. Model-free kinetics analysis of thermal degradation of polysiloxane lubricant. Chem Biochem Eng. 2009;23(4):493–6.

28. Syam Prasad N, Varma KBR. Crystallization kinetics of the LiBO$_2$–Nb$_2$O$_5$ glass using differential thermal analysis. J Am Ceram Soc. 2005;88:357–61.

29. Doyle CD. Kinetic analysis of thermogravimetric data. J Appl Polym Sci. 1961;5:285–92.

30. Sestak J. Thermophysical properties of solids, their measurements and theoretical analysis, vol. 12D. Amsterdam: Elsevier; 1984.

31. Ozawa T. A new method of analyzing thermogravimetric data. Bull Chem Soc Jpn. 1965;38:1881–6.

32. Flyn JH, Wall LA. General treatment of the thermogravimetry of polymers. J Res Nat Bur Stand. 1966;70A:487–523.

33. Yang Q, Jiang Z. The study of criterion for glass crystallization kinetics. J Chin Ceram Soc. 1994;22:419–26.

34. Imran MMA. Crystallization kinetics, glass transition kinetics, and thermal stability of Se$_{70-x}$Ga$_{30}$In$_x$ (x = 5,10,15 and 20) semiconducting glasses. Physica B. 2011;406(3):482–7.

35. Speyer RF. Kinetics of phase transformations in amorphous materials by DSC. Part I. Thermochim Acta. 1988;131:211–24.

36. Augis JA, Bennett JE. Calculation of the Avrami parameters for heterogeneous solid state reactions using a modification of the Kissinger method. J Therm Anal. 1978;13:283–92.

37. Zhang LY, Li H, Hu LL. Statistical structure analysis of GeO$_2$ modified Yb^{3+}: phosphate glasses based on Raman and FTIR study. J Alloys Compd. 2017;698:103–13.

38. Kumar S, Murugavel S, Rao KJ. Absence of germanate anomaly in ternary lithium germanophosphate glasses: modification behavior of mixed glass system of strong and fragile formers. J Phys Chem B. 2001;105:5862–73.

39. Shibata N, Horigudhi M, Edahiro T. Raman spectra of binary high-silica glasses and fibers containing GeO$_2$, P$_2$O$_5$ and B$_2$O$_3$. J Non Cryst Solids. 1981;45:115–26.

40. Francisco BE, Stoldt CR. Energetics ion transport in NASICON-type electrolytes. J Phys Chem C. 2015;119:16432–42.

41. Plotnichenko VG, Sokolov VO, Koltashev VV, Dianov EM. On the structure of phosphosilicate glasses. J Non Cryst Solids. 2002;306:209–26.